Supplementary Figure 1. *Cellular and nuclear ploidy distribution related to the age of the patient*. (A) Violin plots representing the distribution of binuclear polyploid hepatocytes (2x2n, 2x≥4n) (left panel) or mononuclear polyploid hepatocytes (4n, ≥8n) (right panel) in NL (normal liver) related to the age of patients. (B) Violin plots representing the distribution of mononuclear polyploid hepatocytes (4n, ≥8n) in NTT (non-tumoral tissue) and TT (HCC tumoral tissue) related to the age of patients. n corresponds to the number of patients analyzed. Data were compared using Mann Whitney Test.

Supplementary Figure 2. *Ploidy spectrum in non tumoral and tumoral liver parenchyma*. (A) Cellular ploidy distribution (2x2n, 2x≥4n) in NL (normal liver), NTT (non-tumoral tissue) and TT (HCC tumoral tissue). (B) Density plot representing the distribution of mononuclear diploid (2n), tetraploid (4n) and highly polyploid (≥8n) hepatocytes in both tumor (n=75) and non-tumor liver tissue samples (n=71).

Supplementary Figure 3. *Nuclear ploidy spectrum and HCC etiologies*. Comparison of the percentage of mononuclear diploid (2n), tetraploid (4n) and highly polyploid (≥8n) hepatocytes in HCCs related to etiologies (HBC, HCV, Hemochromatosis, Alcohol, Metabolic Syndrome). n corresponds to the number of patients analyzed. Data were compared using MANOVA.

Supplementary Figure 4. *Nuclear ploidy spectrum and HCC molecular features*. Comparison of the percentage of mononuclear diploid (2n), tetraploid (4n) and highly polyploid (≥8n) hepatocytes in HCCs mutated (M) or non mutated (NM) for *ALBUMIN*, *AXIN1*, *ARID1A* and *ARID2*. n corresponds to the number of patients analyzed. Data were compared using MANOVA.

Supplementary Figure 5. *Nuclear ploidy spectrum of HCCs mutated for TERT* promoter, *CTNBB1 and TP53*. Comparison of the percentage of mononuclear diploid (2n), tetraploid (4n) and highly polyploid (≥8n) hepatocytes in HCCs mutated (M) for *TERT* promoter, *CTNNB1*, and *TP53*. n corresponds to the number of patients analyzed. Data were compared using MANOVA.

Supplementary Figure 6. *Nuclear ploidy spectrum and overall survival of patients with HCCs*. (A) Representative higher magnification images (poorly polyploid and highly polyploid tumors) of nuclear ploidy spectrum related to figure 4A. Nuclei are artificially colored according to their ploidy content: 2n/purple, 4n/green, ≥8n/red. (B) Overall survival probability (OSS at 2 and 5 years) in patients with HCCs. Data were compared using Kaplan-Meier curves with log-rank test.

Supplementary Figure 7. Spectrum of *TP53* mutations in highly and poorly mononuclear polyploid tumors. Lolliplot represents the spectrum of somatic mutations in the *TP53* and protein domains of p53. Mutations in highly and poorly polyploid tumors are shown at the top and bottom of the figure, respectively. Frameshift mutations are presented as red circles, nonsense mutations as purple circles, missense mutations as green circles and mutations within splice site sequences as blue circles. Protein domains are indicated in red (transactivation domain), blue (DNA-binding domain) and brown (tetramerisation domain).

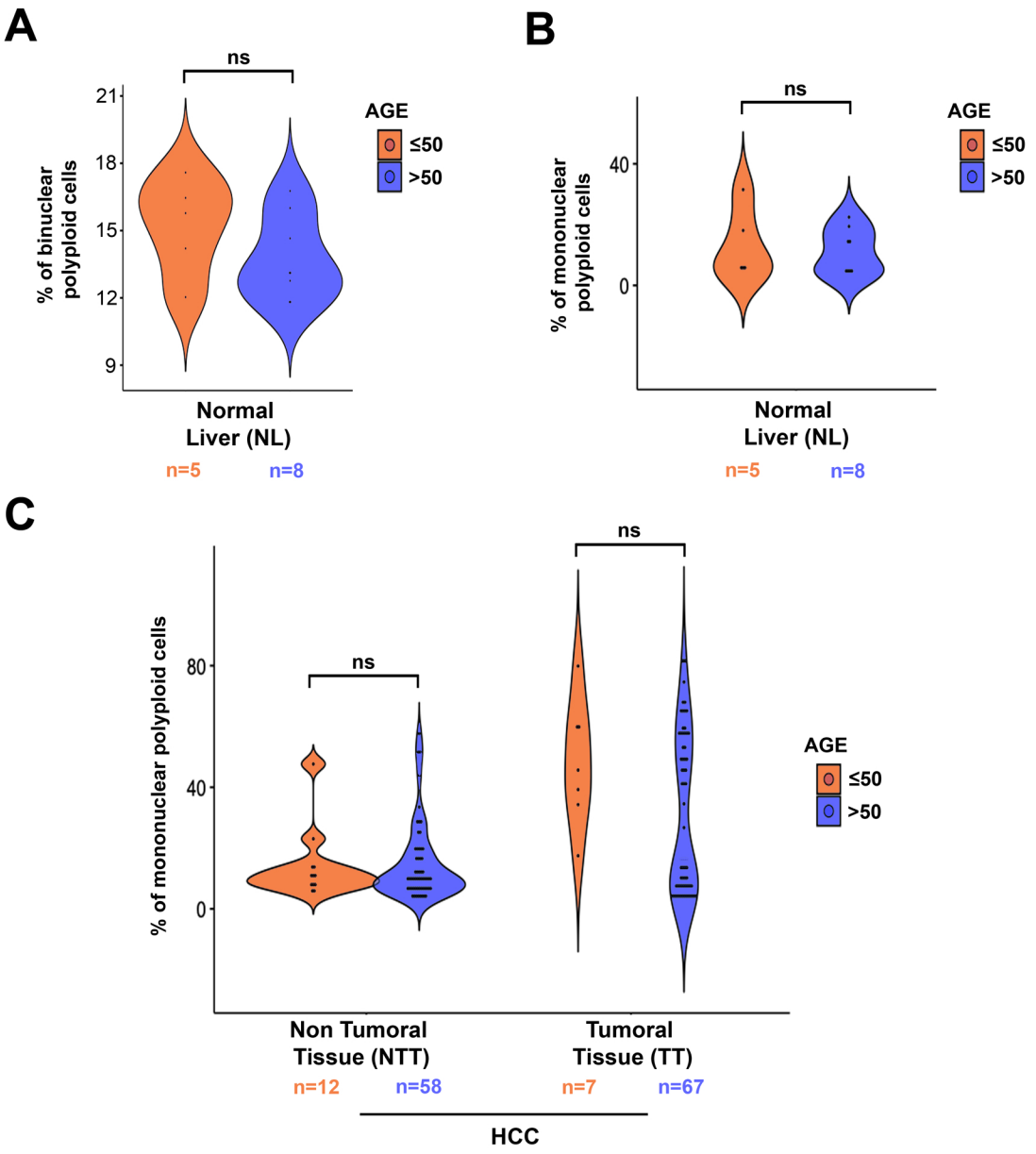

Bou Nader et al. Figure S1

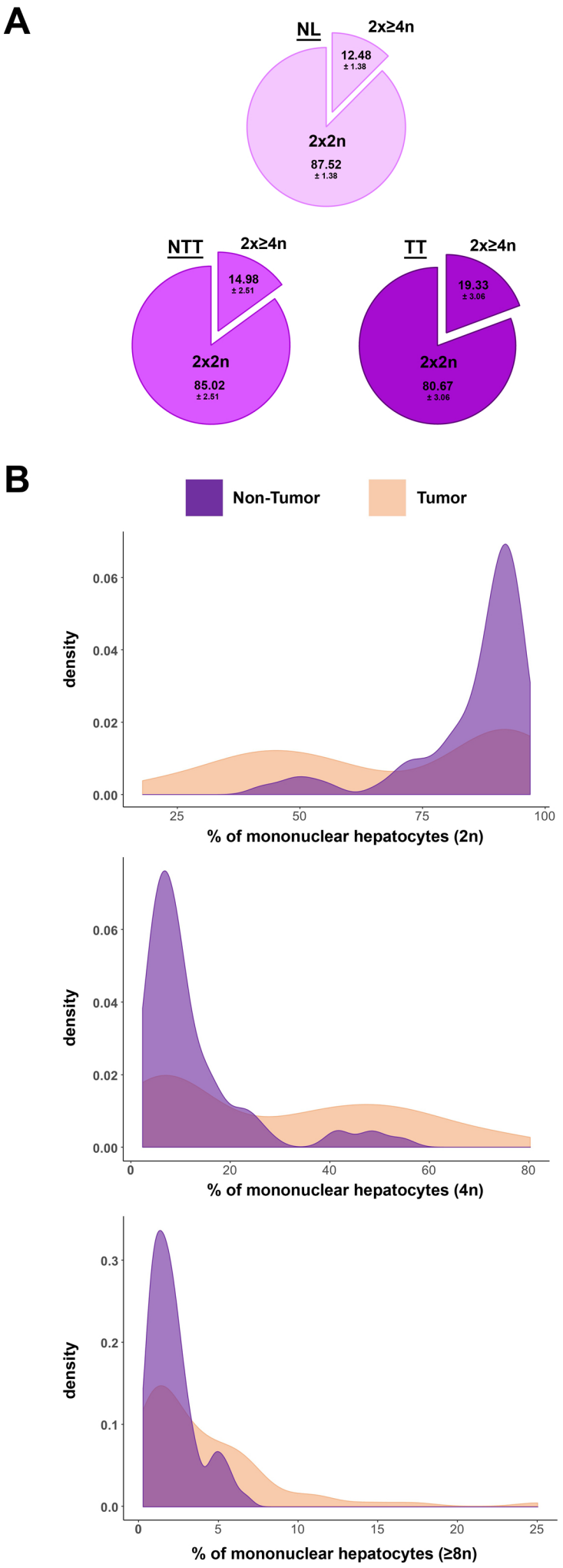

Bou Nader et al. Figure S2

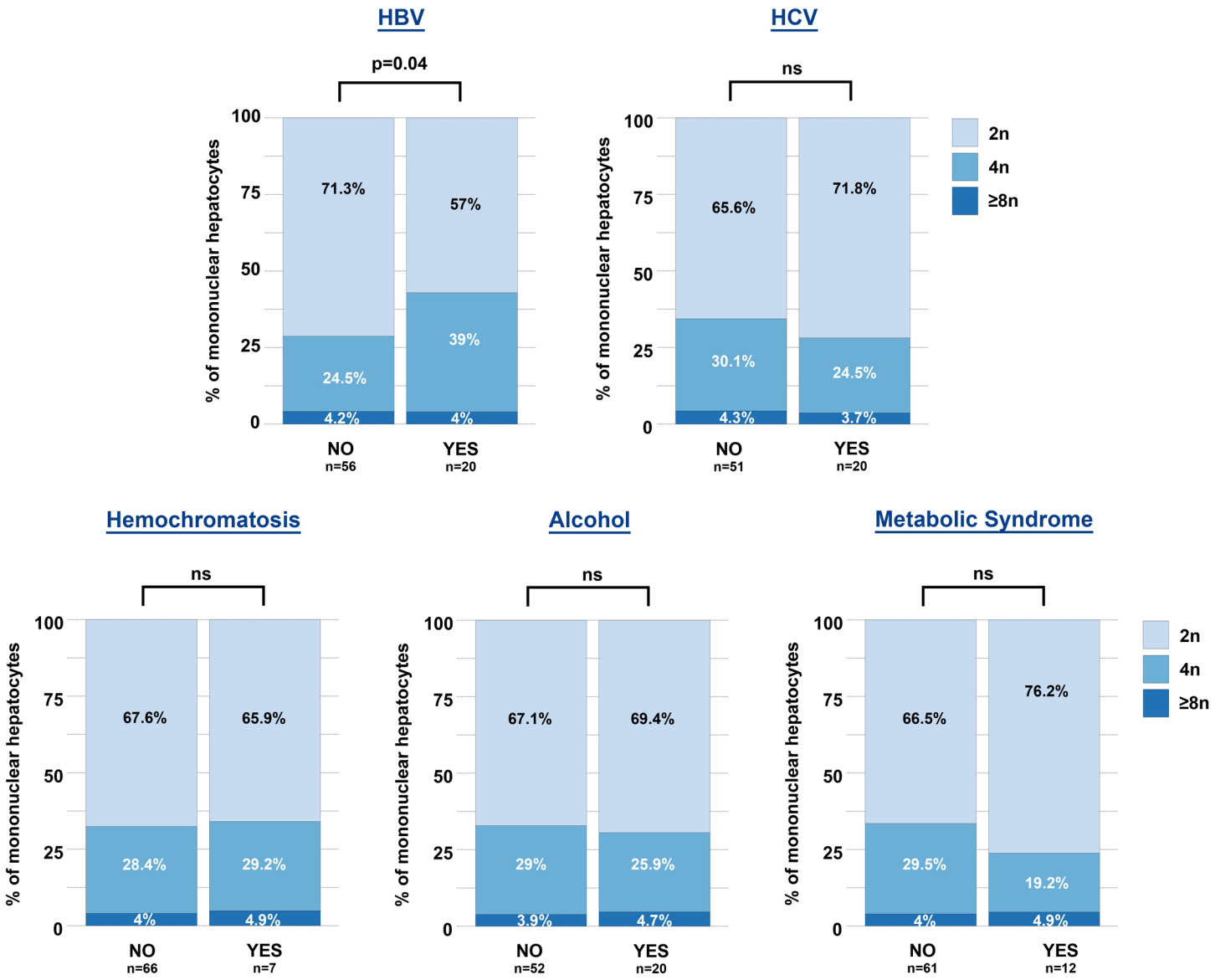

Bou Nader et al. Figure S3

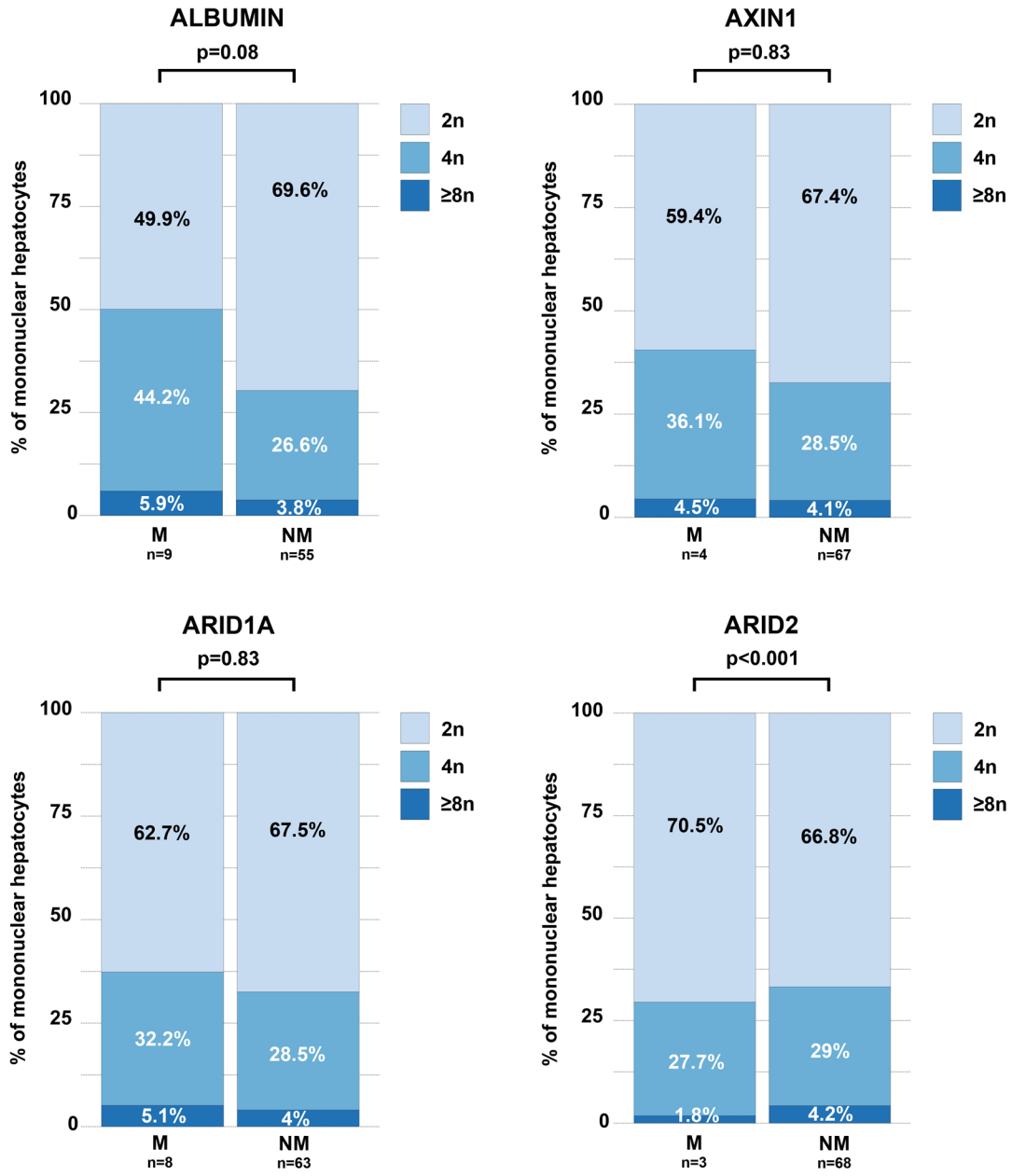

Bou Nader et al. Figure S4

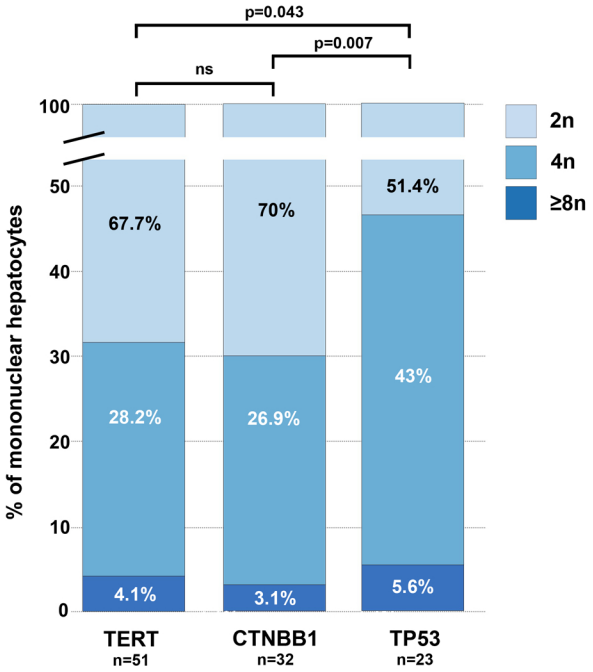

Bou Nader et al. Figure S5

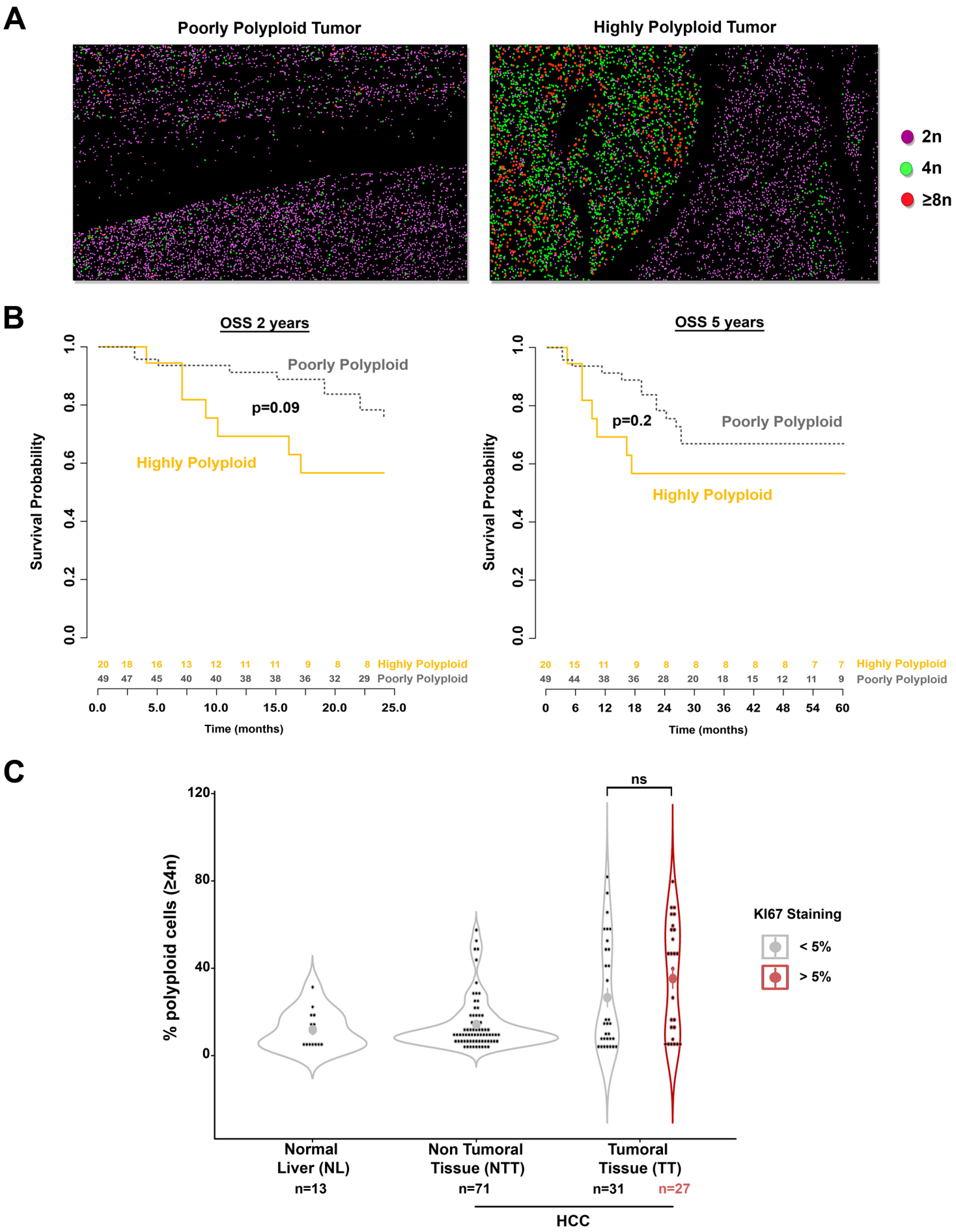

Bou Nader et al. Figure S6

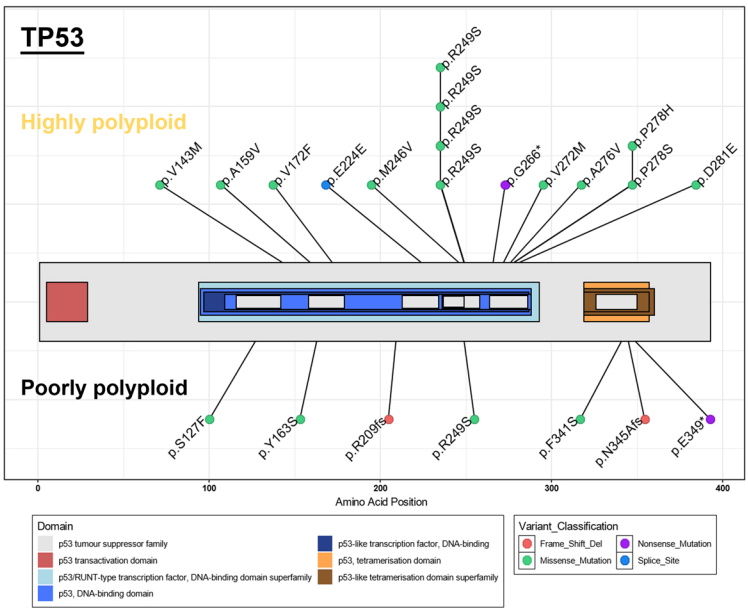

#ID	Hugo_Symbol	CHROM	POS_hg19	REF	ALT	Protein_Change	Variant_Classification	Polyploidy
#1151T	TP53	chr17	7577534	C	A	p.R249S	Missense	High
#1163T	TP53	chr17	7577095	G	T	p.D281E	Missense	High
#1194T	TP53	chr17	7577545	T	C	p.M246V	Missense	High
#1704T	TP53	chr17	7577534	C	A	p.R249S	Missense	High
#1708T	TP53	chr17	7578454	G	A	p.A159V	Missense	High
#1720T	TP53	chr17	7576919	GGGCAGTGC TAGGAAAGA	-	p.?	Splice_Site	High
#1736T	TP53	chr17	7578550	G	A	p.S127F	Missense	Poor
#1739T	TP53	chr17	7578416	C	A	p.V172F	Missense	High
#1742T	TP53	chr17	7577142	C	A	p.G266*	Nonsense	High
#1746T	TP53	chr17	7578176	C	A	p.?	Splice_Site	High
#1747T	TP53	chr17	7573982	C	A	p.E349*	Nonsense	Poor
#1754T	TP53	chr17	7577534	C	A	p.R249S	Missense	Poor
#1756T	TP53	chr17	7577106	G	A	p.P278S	Missense	High
#1756T	TP53	chr17	7577111	G	A	p.A276V	Missense	High
#1764T	TP53	chr17	7573955	CCTTCCCAGC CTGGGCATCC TTGAGTTCCA AGGCCTCATT C	-	p.N345Afs	Frame_Shift	Poor
#1989T	TP53	chr17	7577534	C	A	p.R249S	Missense	High
#1994T	TP53	chr17	7578177	C	T	p.E224E	Splice_Site	High
#2000T	TP53	chr17	7577534	C	A	p.R249S	Missense	High
#3803T	TP53	chr17	7578442	T	G	p.Y163S	Missense	Poor
#3803T	TP53	chr17	7578221	TC	-	p.R209fs	Frame_Shift	Poor
#3837T	TP53	chr17	7577105	G	T	p.P278H	Missense	High
#3843T	TP53	chr17	7577124	C	T	p.V272M	Missense	High
#3854T	TP53	chr17	7578503	C	T	p.V143M	Missense	High
#3867T	TP53	chr17	7574005	A	G	p.F341S	Missense	Poor

Bou Nader et al. Figure S7